Published for SISSA by Springer

Received: June 4, 2021
Revised: November 6, 2021
Accepted: January 10, 2022
Published: February 1, 2022

The breakdown of magneto-hydrodynamics near AdS_2 fixed point and energy diffusion bound

Hyun-Sik Jeong,[a,b] **Keun-Young Kim**[c,d] **and Ya-Wen Sun**[a,b]

[a] *School of Physics & CAS Center for Excellence in Topological Quantum Computation, University of Chinese Academy of Sciences, Zhongguancun east road 80, Beijing 100049, China*

[b] *Kavli Institute for Theoretical Sciences, University of Chinese Academy of Sciences, Zhongguancun east road 80, Beijing 100049, China*

[c] *Department of Physics and Photon Science, Gwangju Institute of Science and Technology, 123 Cheomdan-gwagiro, Gwangju 61005, Korea*

[d] *Research Center for Photon Science Technology, Gwangju Institute of Science and Technology, 123 Cheomdan-gwagiro, Gwangju 61005, Korea*

E-mail: hyunsik@ucas.ac.cn, fortoe@gist.ac.kr, yawen.sun@ucas.ac.cn

Abstract: We investigate the breakdown of magneto-hydrodynamics at low temperature (T) with black holes whose extremal geometry is $AdS_2 \times R^2$. The breakdown is identified by the equilibration scales (ω_{eq}, k_{eq}) defined as the collision point between the diffusive hydrodynamic mode and the longest-lived non-hydrodynamic mode. We show (ω_{eq}, k_{eq}) at low T is determined by the diffusion constant D and the scaling dimension $\Delta(0)$ of an infra-red operator: $\omega_{eq} = 2\pi T\Delta(0)$, $k_{eq}^2 = \omega_{eq}/D$, where $\Delta(0) = 1$ in the presence of magnetic fields. For the purpose of comparison, we have analytically shown $\Delta(0) = 2$ for the axion model independent of the translational symmetry breaking pattern (explicit or spontaneous), which is complementary to previous numerical results. Our results support the conjectured universal upper bound of the energy diffusion $D \leq \omega_{eq}/k_{eq}^2 := v_{eq}^2\,\tau_{eq}$ where $v_{eq} := \omega_{eq}/k_{eq}$ and $\tau_{eq} := \omega_{eq}^{-1}$ are the velocity and the timescale associated to equilibration, implying that the breakdown of hydrodynamics sets the upper bound of the diffusion constant D at low T.

Keywords: Gauge-Gravity Correspondence, Holography and Condensed Matter Physics (AdS/CMT)

ArXiv ePrint: 2105.03882

https://doi.org/10.1007/JHEP02(2022)006

JHEP02(2022)006

Contents

1 Introduction **1**

2 Holographic setup **3**
- 2.1 Model 3
- 2.2 Hydrodynamic mode 4
- 2.3 The determinant method 4

3 Breakdown of magneto-hydrodynamics **6**
- 3.1 Infra-red modes 6
- 3.2 Non-hydrodynamic poles and the collision 8
- 3.3 The breakdown of magneto-hydrodynamics. 10

4 Comparison with the axion model **12**

5 Conclusion **14**

A Axion model **16**
- A.1 Holographic setup 16
- A.2 Gauge-invariant perturbations 17
- A.3 Near-horizon perturbation equations 18

JHEP02(2022)006

1 Introduction

Hydrodynamics is an effective theory for describing near-equilibrium phenomena at late time and large distances [1]. It is constructed by conservation equations together with constitutive relations in a gradient expansion around equilibrium: in the Fourier space, the expansion is in the frequency ω and momentum k. The gradient expansion reflects that hydrodynamics is an effective description of the system at length scales larger than the characteristic length of the system and, at late times, the dynamics of the system back to equilibrium is dominated by the longest-lived mode referred to as hydrodynamic modes.

One may expect that, as higher orders are considered in the expansion, hydrodynamics will be a more precise description for the near equilibrium physics. For instance, one can schematically write the constitutive relation for the stress tensor as

$$T^{\mu\nu} = O(\phi) + O(\nabla\phi) + \dots , \tag{1.1}$$

where ϕ denotes the hydrodynamic variables (such as temperature, fluid velocity). The leading order $O(\phi)$ gives rise to the perfect fluid and the approximation will be improved by the next order expansion $O(\nabla\phi)$ to contain the viscous effect: the viscous fluid.

As in other perturbative expansions, one may ask about the convergence of the hydrodynamic expansion such as "does the hydrodynamic expansion indeed converge?" In

recent years, regarding this question, the breakdown of hydrodynamics has been investigated in [2–14].

In particular, using holography (or the gauge/gravity duality) [15–17], one can characterize the breakdown of hydrodynamics by the equilibration scales $(\omega_{\rm eq}, k_{\rm eq})$ defined as the collision point in the complex (ω, k) space between the hydrodynamic mode and the first-non hydrodynamic mode [12, 13]. At such scales, the lifetime of the non-hydrodynamic mode is comparable to the one of the hydrodynamic mode so that the dynamics of the system can no longer be dominated just by a hydrodynamic mode.

In this work, following previous studies [12, 13], we further study the breakdown of hydrodynamics at low temperature (T) where the black hole has an extremal $\mathrm{AdS}_2\times \mathrm{R}^2$ geometry.[1] In particular, we will see if the following results (1.2)–(1.3) found in previous studies still hold at finite magnetic fields, i.e., we study the breakdown of magneto-hydrodynamics in holography [18–26].[2]

Result 1:

$$\omega_{\rm eq} \;\to\; 2\pi T\Delta(0) \quad \text{as} \quad T\to 0\,, \tag{1.2}$$

where $\Delta(0)$ is the scaling dimension of an infra-red operator at zero wave vector (e.g., (3.10)). This result shows that the non-hydrodynamic mode is related to the infra-red Green's function so that the breakdown at low T is associated to the emergence of the $\mathrm{AdS}_2\times\mathrm{R}^2$ geometry.

Result 2:

$$k_{\rm eq}^2 \;\to\; \frac{\omega_{\rm eq}}{D} \quad \text{as} \quad T\to 0\,, \tag{1.3}$$

which reflects the fact that, at low T, the hydrodynamic dispersion with diffusion constant D at the quadratic order (2.9) in the absolute value becomes a good approximation even at $(\omega_{\rm eq},\ k_{\rm eq})$.[3] From these results, one may simply determine the scales at which hydrodynamics break down from the diffusion constant D and the scaling dimension $\Delta(0)$.

Rearranging (1.3), one can notice that the diffusion constant D at low T can be determined by the breakdown of hydrodynamics $(\omega_{\rm eq},\ k_{\rm eq})$ and can be expressed further as follows

$$D \;\to\; \frac{\omega_{\rm eq}}{k_{\rm eq}^2} \;:=\; v_{\rm eq}^2\,\tau_{\rm eq} \quad \text{as} \quad T\to 0\,, \tag{1.4}$$

where $v_{\rm eq} := \omega_{\rm eq}/k_{\rm eq}$ and $\tau_{\rm eq} := \omega_{\rm eq}^{-1}$ are the velocity and the timescale associated with equilibration [12, 13]. In this velocity and time scales, it turned out (1.4) corresponds to the upper bound of D [12, 13], i.e.,

$$D \;\le\; v_{\rm eq}^2\,\tau_{\rm eq}\,, \tag{1.5}$$

[1] Low temperature states dual to the $\mathrm{AdS}_2\times\mathrm{R}^2$ geometry are related to the Sachdev-Ye-Kitaev (SYK)-like models in strange metals. One can see the breakdown of hydrodynamics of such black holes gives the consistent results with SYK model in [12].

[2] For the recent development of magneto-hydrodynamics, see also [27–29] and references therein.

[3] This may imply that the radius of convergence could be determined by the leading order term in the hydrodynamic expansion [12].

JHEP02(2022)006

where the upper bound (an equality) is approached at low T (1.4). Thus, the breakdown of hydrodynamics can be used to set the upper bound of the diffusion constant D. In this work, in addition to (1.2)–(1.3), we will also study if the conjectured upper bound (1.5) still hold at finite magnetic fields.

Last but not least, our work is related to one of future works proposed in [12]: the investigation of (1.2)–(1.5) with magnetic fields. They studied the breakdown of the energy diffusive hydrodynamics with axion charge (or chemical potential), and found $\Delta(0) = 2$ for those cases. We will study if (1.2)–(1.5) continues to hold for AdS_2 fixed points supported by a different hierarchy of scales for the energy diffusion (i.e., magnetic fields) and identify a corresponding $\Delta(0)$.

Furthermore, we will present how to obtain $\Delta(0)$ analytically using the infra-red Green's function at finite magnetic fields. Using the same procedure, for the purpose of the comparison with previous studies, we will also show the analytic expression of $\Delta(0)$ for the general axion models (A.1), which is consistent with previous numerical results [13].

This paper is organized as follows. In section 2, we introduce the holographic model with magnetic fields and present the determinant method for the quasi-normal modes. In section 3, we study the breakdown of magneto-hydrodynamics with the quasi-normal mode computations and determine $(\omega_{\rm eq}, k_{\rm eq})$. We also show how to obtain $\omega_{\rm eq}$ analytically from the infra-red Green's function. In section 4 we compare our results with the previous study of the breakdown of energy diffusive hydrodynamics [12]. Section 5 is devoted to conclusions.

2 Holographic setup

2.1 Model

We consider the Einstein-Maxwell system in (3+1) dimensions

$$S = \int \mathrm{d}^4x\sqrt{-g}\left(R + 6 - \frac{1}{4}F^2\right), \tag{2.1}$$

with a background metric

$$\mathrm{d}s^2 = -f(r)\,\mathrm{d}t^2 + \frac{1}{f(r)}\,\mathrm{d}r^2 + r^2(\mathrm{d}x^2+\mathrm{d}y^2), \quad A = -\frac{H}{2}y\,\mathrm{d}x + \frac{H}{2}x\,\mathrm{d}y, \tag{2.2}$$

where H is the external magnetic field that breaks translational invariance. The blackening factor $f(r)$ is

$$f(r) = r^2 - \frac{m_0}{r} + \frac{H^2}{4\,r^2}, \quad m_0 = r_h^3\left(1+\frac{H^2}{4\,r_h^4}\right), \tag{2.3}$$

where m_0 is determined by the condition $f(r_h) = 0$.

Thermodynamic quantities [30] including the Hawking temperature T read

$$T = \frac{1}{4\pi}\left(3\,r_h - \frac{H^2}{4\,r_h^3}\right), \quad \epsilon = 2\,r_h^3 + \frac{H^2}{2\,r_h}, \quad P = r_h^3 - \frac{3H^2}{4\,r_h}, \quad s = 4\pi r_h^2, \tag{2.4}$$

where (ϵ, P, s) are the energy density, pressure, and entropy density respectively. Note that these quantities satisfy the following Smarr-like relation as

$$\epsilon + P = s\,T. \tag{2.5}$$

JHEP02(2022)006

2.2 Hydrodynamic mode

We can study the holographic dual of hydrodynamic modes of (2.1) with the fluctuations

$$g_{\mu\nu} \to g_{\mu\nu} + \delta g_{\mu\nu}\,, \quad A_\mu \to A_\mu + \delta A_\mu\,. \tag{2.6}$$

At the linearized fluctuation level of the Einstein equations and the Maxwell equation, one can find two sets of decoupled fluctuations:

$$\begin{aligned} &\text{(Sound channel):} \quad \{\delta g_{tt},\, \delta g_{tx},\, \delta g_{xx},\, \delta g_{yy},\, \delta A_y\}\,, \\ &\text{(Shear channel):} \quad \{\delta g_{ty},\, \delta g_{xy},\, \delta A_t,\, \delta A_x\}\,. \end{aligned} \tag{2.7}$$

In this paper, we focus on the sound channel related to the energy diffusion mode with the wave vector in the x-direction:

$$\begin{aligned} &\delta g_{tt} = h_{tt}(r)\, e^{-i\omega t + i k x}\,, \quad \delta g_{tx} = h_{tx}(r)\, e^{-i\omega t + i k x}\,, \quad \delta g_{xx} = h_{xx}(r)\, e^{-i\omega t + i k x}\,, \\ &\delta g_{yy} = h_{yy}(r)\, e^{-i\omega t + i k x}\,, \quad \delta A_y = a_y(r)\, e^{-i\omega t + i k x}\,. \end{aligned} \tag{2.8}$$

At finite magnetic fields, (2.1) produces the quasi-normal modes well matched with the magneto-hydrodynamics. See [31] for more details as well as the review of the magneto-hydrodynamics.

The hydrodynamic mode of the sound channel (2.8) corresponds to the energy diffusive mode at the small k limit as

$$\omega = -i\, D\, k^2\,. \tag{2.9}$$

The energy diffusion constant D is given [31–33] as

$$D := \frac{\kappa}{c_\rho}\,, \quad \kappa = \frac{s^2\, T}{H^2}\,, \quad c_\rho := T\frac{\partial s}{\partial T}\,, \tag{2.10}$$

where κ is the thermal conductivity and c_ρ is the specific heat. Moreover, using

$$\frac{\partial s}{\partial T} = (8\pi r_h)\frac{\partial r_h}{\partial T}\,, \quad \frac{\partial r_h}{\partial T} = \frac{16\pi r_h^4}{12 r_h^4 + 3H^2}\,, \tag{2.11}$$

we can express the energy diffusion constant[4] as

$$D = \frac{3 r_h^3}{2H^2} + \frac{3}{8 r_h}\,. \tag{2.12}$$

2.3 The determinant method

The determinant method for the magnetically charged black hole is given in [31]. For the convenience of the reader, we also present it as follows.

[4]This diffusion constant becomes the same as $\frac{\partial P}{\partial \epsilon}\frac{\epsilon+P}{\sigma_Q H^2}$ in the small H/T^2 limit, where the first-order transport coefficient $\sigma_Q = 1$ in small H/T^2 limit. See [31].

JHEP02(2022)006

Gauge-invariant perturbation: in order to study the energy diffusion mode (2.9) at finite magnetic fields, we can choose the following diffeomorphisms and gauge-invariant combinations [18, 19]:

$$\begin{aligned} Z_H &:= \frac{4k}{\omega}\, h^x_t \,+\, 2h^x_x - \left(2 - \frac{k^2}{\omega^2}\frac{f'(r)}{r}\right) h^y_y + \frac{2k^2}{\omega^2}\frac{f(r)}{r^2} h^t_t \,, \\ Z_A &:= a_y \,+\, \frac{iH}{2k}\left(h^x_x - h^y_y\right) \,, \end{aligned} \tag{2.13}$$

where an index on metric fluctuations is raised with the background metric (2.2). Then we can obtain two field equations for Z_H and Z_A:

$$\begin{aligned} 0 \,&=\, A_H\, Z''_H \,+\, B_H\, Z'_H \,+\, C_H\, Z_H \,+\, D_H\, Z'_A \,+\, E_H\, Z_A \,, \\ 0 \,&=\, A_A\, Z''_A \,+\, B_A\, Z'_A \,+\, C_A\, Z_A \,+\, D_A\, Z'_H \,+\, E_A\, Z_H \,. \end{aligned} \tag{2.14}$$

In order to avoid clutter, we will not write the coefficients of equations in the paper.

In order to study the quasi-normal mode spectrums, we need to solve the equations of motion (2.14) with boundary conditions: one from the horizon ($r \to r_h$) and the other from the AdS boundary ($r \to \infty$).

Near the horizon, the variables can be expanded as

$$\begin{aligned} Z_H &= (r - r_h)^{\nu_\pm} \left(Z^{(I)}_H \,+\, Z^{(II)}_H (r - r_h) \,+\, \dots\right) \,, \\ Z_A &= (r - r_h)^{\nu_\pm} \left(Z^{(I)}_A \,+\, Z^{(II)}_A (r - r_h) \,+\, \dots\right) \,, \end{aligned} \tag{2.15}$$

where $\nu_\pm := \pm i\omega/4\pi T$ and we choose $\nu_- := -i\omega/4\pi T$ for the incoming boundary condition. One can check that there are two independent horizon variables $(Z^{(I)}_H, Z^{(I)}_A)$ and higher order coefficients are determined by them.

On the other hand, near the AdS boundary, the asymptotic behavior of variables are

$$\begin{aligned} Z_H &= Z^{(S)}_H\, r^0\, (1 \,+\, \dots) \,+\, Z^{(R)}_H\, r^{-3}\, (1 \,+\, \dots) \,, \\ Z_A &= Z^{(S)}_A\, r^0\, (1 \,+\, \dots) \,+\, Z^{(R)}_A\, r^{-1}\, (1 \,+\, \dots) \,, \end{aligned} \tag{2.16}$$

where the superscript (S) refers to the source term while (R) denotes the response term.

The determinant method: now we can compute the quasi-normal modes by employing the determinant method [34]. The determinant method is related to the source terms near the AdS boundary. For instance, by the shooting method, one can construct the 2×2 S-matrix as:

$$S = \begin{pmatrix} Z^{(S)(I)}_H & Z^{(S)(II)}_H \\ Z^{(S)(I)}_A & Z^{(S)(II)}_A \end{pmatrix} \,. \tag{2.17}$$

Since we have two independent shooting variables at the horizon (2.15), we can obtain two independent solutions so that S-matrix (2.17) becomes a 2×2 matrix. Note that $I(II)$ in (2.17) indicates that the each column is obtained by the $I(II)$-th shooting.

Finally, one can find the quasi-normal mode spectrum by the value (ω, k) in which the determinant of (2.17) is vanishing.

JHEP02(2022)006

3 Breakdown of magneto-hydrodynamics

3.1 Infra-red modes

In this section, we study the perturbation equation (2.14) in the $\mathrm{AdS}_2 \times \mathrm{R}^2$ spacetime that emerges near the horizon at low temperatures. We will closely follow the method given in the appendix A in [12].

By solving the perturbation equation in the extremal geometry (near the horizon at low temperature), we will obtain the infra-red Green's function $\mathcal{G}_{\mathrm{IR}}$ analytically with an operator of dimension $\Delta(k)$ at the infra-red fixed point of the field theory. From this analysis, we will show that the analytic equilibration frequency ω_{eq} at low temperature is

$$\omega_{\mathrm{eq}} \,=\, 2\pi T\, \Delta(k=0)\,. \tag{3.1}$$

The extremal geometry. Let us first discuss the small temperature condition. From (2.4), one can check that the temperature becomes zero ($T=0$) at

$$r_h = r_e\,, \quad r_e := \left(\frac{H}{\sqrt{12}}\right)^{1/2}\,. \tag{3.2}$$

Thus, by putting the following relation into the Hawking temperature in (2.4)

$$T \,=\, 0 \,+\, \epsilon\, \delta T\,, \quad r_h \,=\, r_e \,+\, \epsilon\, \zeta_h\,, \tag{3.3}$$

and take $\epsilon \to 0$, we can find the small temperature correction ζ_h as

$$\zeta_h \,=\, \frac{\pi}{3}\delta T\,. \tag{3.4}$$

Next, in order to obtain the extremal geometry, one can consider the following coordinate transformation [12, 35] in (2.2)

$$r \,=\, r_e \,+\, \epsilon\, \zeta\,, \quad r_h \,=\, r_e \,+\, \epsilon\, \zeta_h\,, \quad t \,=\, \frac{u}{\epsilon}\,, \tag{3.5}$$

and take $\epsilon \to 0$. Then we can change the coordinate from (t, r) to (u, ζ) as follows

$$\mathrm{d}s^2 = -\frac{\zeta^2}{L^2}\left(1-\frac{\zeta_h}{\zeta}\right)^2 \mathrm{d}u^2 + \frac{L^2}{\zeta^2\left(1-\frac{\zeta_h}{\zeta}\right)^2}\,\mathrm{d}\zeta^2 + r_e^2(\mathrm{d}x^2+\mathrm{d}y^2)\,, \tag{3.6}$$

where the AdS_2 radius of curvature is $L^2 = 1/6$. Note that this geometry corresponds to the $\mathrm{AdS}_2 \times \mathrm{R}^2$ geometry with the small temperature correction (ζ_h), and ζ runs from $\zeta = \zeta_h$ to $\zeta = \infty$ (the AdS_2 boundary).

The perturbation equation in the extremal geometry. Using the following coordinate transformation,

$$r \,=\, r_e \,+\, \epsilon\, \zeta\,, \quad r_h \,=\, r_e \,+\, \epsilon\, \zeta_h\,, \quad \omega \,=\, \epsilon\, \zeta_\omega\,, \tag{3.7}$$

we can obtain the perturbation equations (2.14) in the extremal geometry (3.6) in the $\epsilon \to 0$ limit. Note that (3.7) is the Fourier transformed version of (3.5).

JHEP02(2022)006

At the leading order in ϵ, one can check only the second perturbation equation in (2.14) survives: the first perturbation equation starts at $\mathcal{O}(\epsilon)$ order. In particular, the survived equation of motion is composed of only one field $Z_A(\zeta)$:

$$\partial_\zeta^2 Z_A + \left(\frac{2\zeta}{\zeta^2-\zeta_h^2}\right)\partial_\zeta Z_A + \left(\frac{\zeta_\omega^2}{36\,(\zeta^2-\zeta_h^2)^2} - \frac{k^2}{\sqrt{3}\,H\,(\zeta^2-\zeta_h^2)}\right) Z_A = 0\,. \tag{3.8}$$

Near the AdS_2 boundary ($\zeta \to \infty$), the solution of the equation is expanded as

$$Z_A \;=\; Z^{(S)}\,\zeta^{\Delta(k)-1} + Z^{(R)}\,\zeta^{-\Delta(k)}\,, \tag{3.9}$$

where the scaling dimension $\Delta(k)$ is

$$\Delta(k) = \frac{1}{2}\left(1+\sqrt{1+\frac{4\,k^2}{\sqrt{3}\,H}}\right)\,. \tag{3.10}$$

The infra-red Green's function: the infra-red Green's function can be found explicitly by solving the equations (3.8) and imposing the usual AdS/CFT rules[5] at the AdS_2 boundary ($\zeta \to \infty$) [35, 36]

$$\mathcal{G}_{\rm IR} \propto \frac{Z^{(R)}}{Z^{(S)}}\,, \tag{3.11}$$

where $Z^{(S)}$, $Z^{(R)}$ are coefficients in (3.9). Let us show the explicit form of the infra-red Green's function

$$\mathcal{G}_{\rm IR} = \frac{2\Delta(k)-1}{2}\left(\frac{6}{\pi}\right)^{1-2\Delta(k)}\delta T^{2\,\Delta(k)-1}\frac{\Gamma\left(\frac{1}{2}-\Delta(k)\right)\Gamma\left(\Delta(k)-\frac{i\zeta_\omega}{2\pi\delta T}\right)}{\Gamma\left(\frac{1}{2}+\Delta(k)\right)\Gamma\left(1-\Delta(k)-\frac{i\zeta_\omega}{2\pi\delta T}\right)}\,. \tag{3.12}$$

From (3.12), the infra-red Green's function, $\mathcal{G}_{\rm IR}$, gives poles along the imaginary frequency axis at the locations

$$\zeta_{\omega,\,n} \;=\; -i\,2\pi\,\delta T\,(n\,+\,\Delta(k))\,, \qquad n\,=\,0,1,2,\ldots\,. \tag{3.13}$$

In order to reconstruct the full retarded Green's function (G^R) analytically, and give the quasi-normal mode beyond the small temperature regime, one must extend the near-horizon solutions through the rest of the spacetime, which is difficult to do. However, for the purpose of studying the low-temperature behavior, it might be enough to observe that G^R exhibits poles from (2.17), where its locations approach those of the poles of $\mathcal{G}_{\rm IR}$ (3.13) as ($k \to 0$, $T \to 0$) [12].[6] In other words, this means that in this limit G^R exhibits poles at

$$\omega_n \;=\; -i\,2\pi\,T\,(n\,+\,\Delta(0))\,, \qquad n\,=\,0,1,2,\ldots\,, \tag{3.14}$$

where $(\omega_n,\,T)$ may approach to $(\zeta_{\omega,\,n}\,,\,\delta T)$ with $\Delta(0)=1$ (3.10). In the next section, we will show this analytic result is consistent with the numerical results of the quasi-normal mode spectrum.

[5] The general solution has the associated Legendre function of the second kind which corresponds to the out-going solution at $\zeta=\zeta_h$, so we should discard it.

[6] Dividing (2.9) with T, we have $\omega/T = -iD\,k^2/T$. Then, the relevant low T limit is ($k \to 0$, $T \to 0$) to keep k^2/T fixed and therefore ω/T fixed. See more details in the appendix A of [12].

JHEP02(2022)006

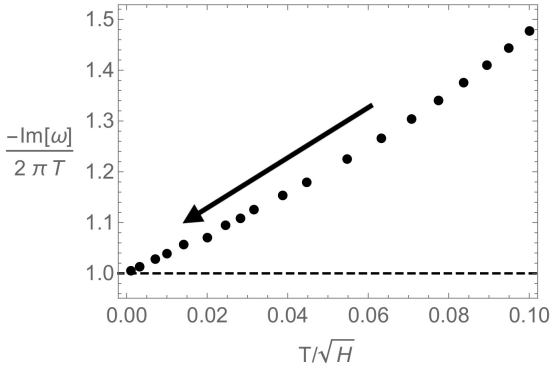

Figure 1. The first non-hydrodynamic mode at $k/T = 1/10$. Black dots are quasi-normal modes and the dashed line is ω_0 (3.14).

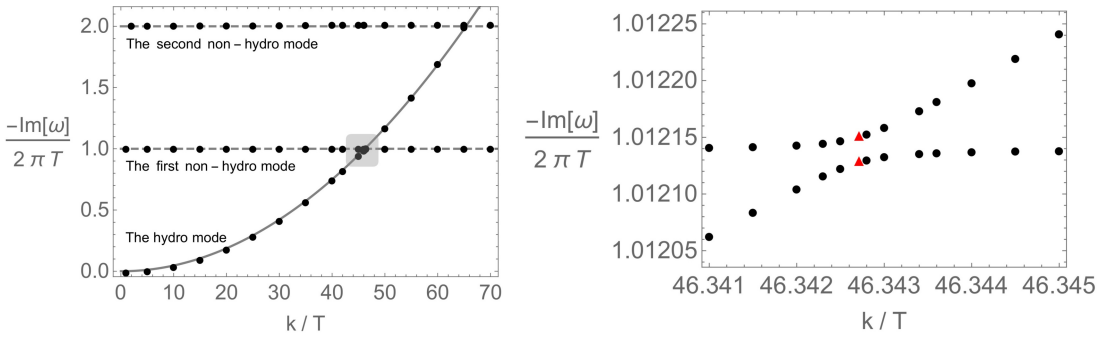

(a) Quasi-normal mode

(b) A zoom of the gray square region

Figure 2. Quasi-normal modes (black dots) at $H/T^2 = 10^5$. *Left:* the solid line is the hydrodynamic mode (2.9) and the dashed line is the non-hydrodynamic mode (3.14). *Right:* a zoomed in figure of the gray square region in figure 2(a).

3.2 Non-hydrodynamic poles and the collision

Non-hydrodynamic modes. In order to study the breakdown of magneto-hydrodynamics, we need to identify the non-hydrodynamic modes whose longest-lived mode (the first non-hydro mode) will make the collision with the hydrodynamic mode.

In particular, as in the hydrodynamic mode (2.9), it is tempting to obtain the expression of the non-hydrodynamic mode in the small wave vector regime. As long as we consider the low temperature regime, it has been discovered the non-hydrodynamic modes follow (3.14) at small wave vector [12, 13], i.e., the origin of the non-hydrodynamic mode at low T is associated to the AdS_2 geometry.

We find this is also valid in the presence of magnetic fields. In figure 1, we display the first non-hydro mode[7] in agreement with ω_0 (3.14) at $T/\sqrt{H} \to 0$, which is responsible for the breakdown of hydrodynamic.

The collision between poles. Next, let us examine how this first non-hydro mode collides with the hydrodynamic mode. In figure 2(a), we first show the quasi-normal modes

[7]The higher non-hydro mode is also well matched with ω_n (3.14).

JHEP02(2022)006

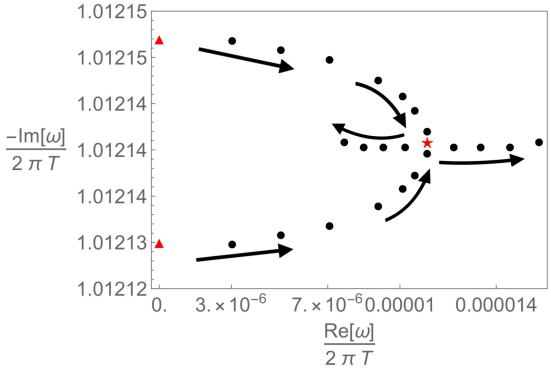

Figure 3. Quasi-normal modes in the complex ω plane as ϕ_k is increased from 0 (red triangles) to 0.0000116 at $H/T^2 = 10^5$ and $|k|/T = 46.342712$. Red triangles are the same as in figure 2(b). Red star indicates the collision point ($\phi_k \sim 0.00001113$).

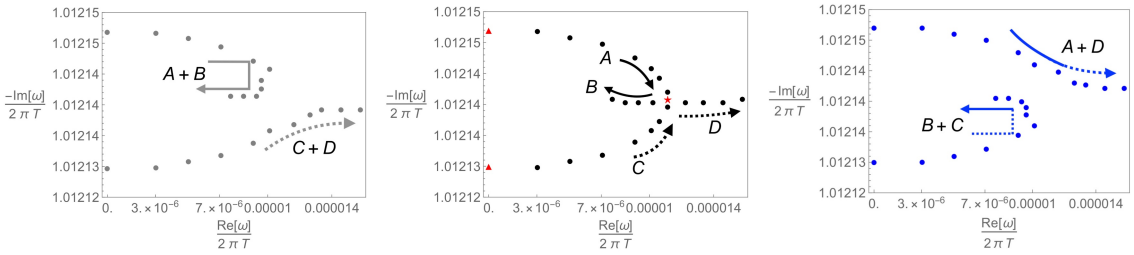

(a) $|k| < |k_c|$ (b) $|k| = |k_c|$ (c) $|k| > |k_c|$

Figure 4. Quasi-normal modes near $|k_c|/T$ at $\phi_k \in [0, 0.0000116]$: $|k|-|k_c| = (-1.2\times10^{-5}, 0, 1.2\times10^{-5})\,T$ (left, center, right).

at low T. One can see the quasi-normal modes (black dots) are well matched with i) the hydrodynamic mode (solid line) (2.9); ii) the non-hydrodynamic mode (dashed line) (3.14).

The gray square region around $k/T \sim 46$ indicates the location in which the collision between the hydro mode and the first non-hydro mode may appear. As we investigate this gray region carefully, one may see the collision cannot be visible in this real k/T plot. We display the zoom of this gray region in figure 2(b): the first non-hydro mode does not collide with the hydro mode where the red triangle will be used as the guide to find the collision point in the following.

In order to find out the collision point (ω_c, k_c), we need to extend the quasi-normal mode analysis into the complex plane [12]. Introducing the phase of k (ϕ_k),

$$k = |k|\, e^{i\,\phi_k}\,, \tag{3.15}$$

we can examine how the poles move in the complex ω plane. In figure 3, we display the poles at $|k|/T = 46.342712$ with changing ϕ_k.[8] As we increase the phase ϕ_k from 0 (red triangles) to 0.0000116, poles make the collision around $\phi_k \sim 0.00001113$ (red star). Note that the red triangles ($\phi_k = 0$) in figure 3 are the same as in figure 2(b), so one may imagine putting one additional axis Re[ω] on figure 2(b) with (3.15), and that would be figure 3.

[8] As ϕ_k approaches 2π, it is expected that the poles become the same poles for $\phi_k = 0$.

JHEP02(2022)006

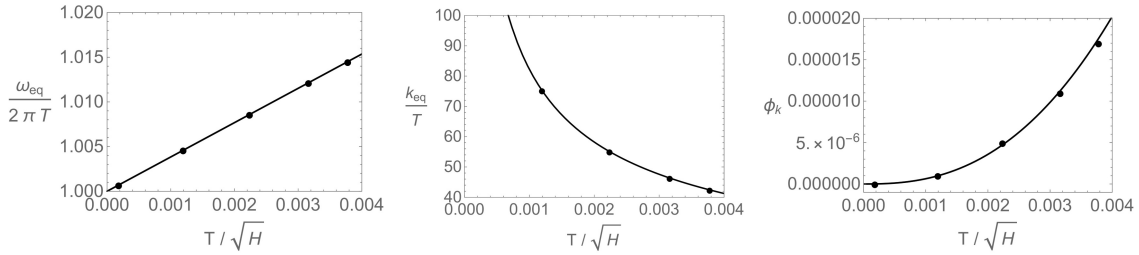

(a) $\omega_{\rm eq}$ vs T (b) $k_{\rm eq}$ vs T (c) ϕ_k vs T

Figure 5. The temperature dependence of $(\omega_{\rm eq},\, k_{\rm eq},\, \phi_k)$. Dots are numerical data and black solid lines are fitting curves (3.17).

The wave number ($|k|/T = 46.342712$) used in figure 3 corresponds to $|k_c|/T$ because of the existence of the collision. Let us further investigate the quasi-normal mode near $|k_c|/T$ in figure 4 and summarize the results as

- $|k| = |k_c|$: figure 4(b), we label (A, B, C, D) for each arrows, which is the same figure as figure 3.
- $|k| < |k_c|$: figure 4(a), one cannot see the collision and A connects to B while C is with D.
- $|k| > |k_c|$: figure 4(c), one also cannot see the collision and A connects to D while C is with B.

3.3 The breakdown of magneto-hydrodynamics.

The collision point $(\omega_{\rm c}, k_{\rm c})$ signals the breakdown of the hydrodynamics and its absolute value is defined as $(\omega_{\rm eq}, k_{\rm eq})$ [12, 13]

$$\omega_{\rm eq} := |\omega_c|\,, \quad k_{\rm eq} := |k_c|\,. \tag{3.16}$$

We show the temperature dependence of the equilibration data $(\omega_{\rm eq},\, k_{\rm eq},\, \phi_k)$ in figure 5 with the fitting curves

$$\frac{\omega_{\rm eq}}{2\pi T} \sim \Delta(0) + \#\, T\,, \qquad \frac{k_{\rm eq}}{T} \sim \frac{\#}{\sqrt{T}}\,, \qquad \phi_k \sim \#\, T^{5/2}\,, \tag{3.17}$$

where $\Delta(0) = 1$ (3.10)[9] and as pointed out in [12], the collision point seems to follow

$$\omega_c = \omega_{\rm eq}\, e^{i(\phi_k - \frac{\pi}{2})}\,, \quad k_c = k_{\rm eq}\, e^{i\phi_k}\,, \tag{3.18}$$

so, as the temperature is lowered, the phase is vanishing and the collision appears at pure imaginary frequency and pure real momentum as

$$\omega_c \to -i\,\omega_{\rm eq}\,, \quad k_c \to k_{\rm eq}\,. \tag{3.19}$$

[9]For the shear diffusion mode [12], it turned out $\Delta(0)$ has the same value as $\Delta(0) = 1$. However, the phase ϕ_k has a different scaling behavior as $\phi_k \sim T^{1/2}$, so the phase seems to depend on the type of the diffusive mode.

JHEP02(2022)006

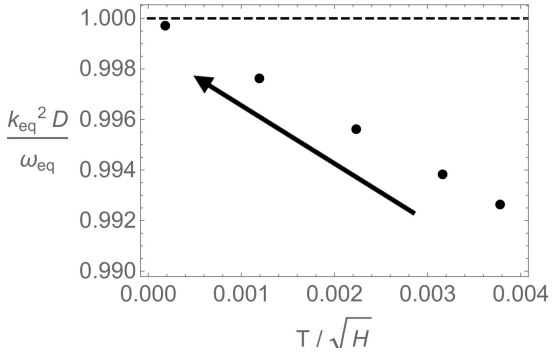

Figure 6. The upper bound on the diffusion constant (2.12). The dashed line indicates the upper bound (3.22).

The upper bound of AdS_2 diffusion with magnetic fields. In holography, it has been studied to find a universal bound for the diffusion constant D, and it turned out D can have a lower bound [37–42][10] with the velocity and the time scales related to quantum chaos

$$D \geq v_{\rm B}^2 \, \tau_{\rm L} \,, \tag{3.20}$$

where $v_{\rm B}$ is a butterfly velocity and $\tau_{\rm L}$ is the Lyapunov time. $(v_{\rm B}, \tau_{\rm L})$ characterize the chaotic behavior [43] via out-of-time-order correlators (OTOCs) [44–46].[11]

In recent years, the holographic study of the "upper" bound has also been investigated with the simple question: the diffusion constant will also be bounded from above or it just grows forever? It is proposed that the diffusion constant D has the following upper bound [12, 13]:

$$D \leq v_{\rm eq}^2 \, \tau_{\rm eq} \,, \tag{3.21}$$

where $v_{\rm eq} := \omega_{\rm eq}/k_{\rm eq}$ and $\tau_{\rm eq} := \omega_{\rm eq}^{-1}$ are the velocity and the timescale associated to the breakdown of hydrodynamics (3.16). The upper bound (an equality) in (3.21) is approached at low T and it can be expressed as

$$\frac{D}{v_{\rm eq}^2 \, \tau_{\rm eq}} = \frac{k_{\rm eq}^2}{\omega_{\rm eq}} D = 1 \,. \tag{3.22}$$

In figure 6, we show that the conjectured inequality (3.21) still holds in the presence of magnetic fields for which the upper bound (3.22) is approached at low T. The appearance of the upper bound implies that we have the following at low T

$$\omega_{\rm eq} = D \, k_{\rm eq}^2 \,, \tag{3.23}$$

and it means, as T is lowered, the quasi-normal modes are well approximated with i) the hydrodynamic mode (2.9); ii) the non-hydrodynamic mode (3.14). See figure 7.

[10] This is the case when the IR geometry is $AdS_2 \times R^2$. There could be a pre-factor when the IR geometry changes.

[11] OTOCs is one useful tool to study many-body quantum chaos: $\langle V_0(0) W_{\mathbf{x}}(t) V_0(0) W_{\mathbf{x}}(t) \rangle \sim 1 + e^{\lambda_L (t - x/v_B)}$ where $\lambda_L := 1/\tau_L$.

JHEP02(2022)006

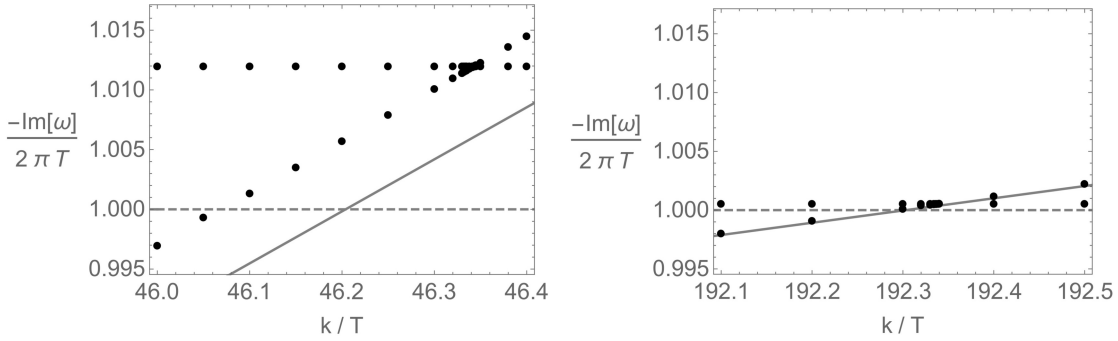

(a) $H/T^2 = 10^5$ (b) $H/T^2 = 3 \times 10^7$

Figure 7. Quasi-normal modes (black dots) at $H/T^2 = (10^5, 3 \times 10^7)$ (left, right). The solid line is the hydrodynamic mode (2.9) and the dashed line is the first non-hydrodynamic mode ω_0 (3.14). Note that the left figure is the gray square region in figure 2(a). As T is lowered from (a) to (b), the quasi-normal modes (black dots) are getting better and better approximated with i) the hydrodynamic mode (solid line); ii) the non-hydrodynamic mode (dashed line).

4 Comparison with the axion model

In this section, we compare our results with the previous study of the equilibration data for the energy diffusion [12] where the energy diffusion is studied with the linear axion model: (A.1) at $N = 1$.[12] We find two main differences: i) $\Delta(0)$ (or the equilibration time $\omega_{\rm eq}$); ii) the T-scaling in the phase ϕ_k.

The operator of dimension $\Delta(0)$. For $\Delta(0)$, the linear axion model gives $\Delta(0) = 2$ unlike the finite magnetic field case $\Delta(0) = 1$ (3.10). We may understand this from the perturbation equation in the extremal geometry as

$$\partial_\zeta^2 Z_A + \left(\frac{2\zeta}{\zeta^2 - \zeta_h^2}\right)\partial_\zeta Z_A + \left(\frac{c_1\,\zeta_\omega^2}{(\zeta^2-\zeta_h^2)^2} - \frac{c_2 + c_3\,k^2}{(\zeta^2-\zeta_h^2)}\right) Z_A = 0\,, \tag{4.1}$$

where c_i are constants depending on the theories:

$$\begin{aligned} \text{Magnetic field model:} \quad & c_1 = \frac{1}{36}\,, \quad c_2 = 0\,, \quad c_3 = \frac{1}{\sqrt{3}H}\,, \\ \text{Linear axion model:} \quad & c_1 = \frac{1}{9}\,, \quad c_2 = 2\,, \quad c_3 = \frac{2}{m^2}\,, \end{aligned} \tag{4.2}$$

where the magnetic field model case is given in (3.8) and the linear axion model case is in (A.12) with $N = 1$.

Near the AdS_2 boundary, the equation (4.1) with (3.9) gives an operator of dimension $\Delta(k)$ as

$$\Delta(k) = \frac{1}{2}\left(1 + \sqrt{(1+4\,c_2) + 4c_3\,k^2}\right)\,, \tag{4.3}$$

[12]The translational invariant system at finite chemical potential [12] gives the same result with the linear axion model so we focus on the linear axion model case here.

JHEP02(2022)006

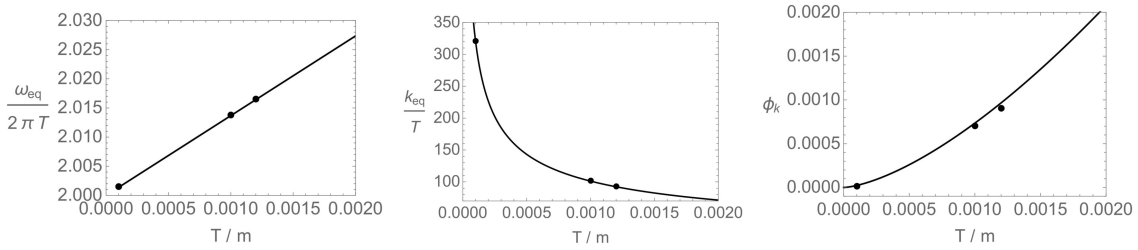

(a) $\omega_{\rm eq}$ vs T (b) $k_{\rm eq}$ vs T (c) ϕ_k vs T

Figure 8. The temperature dependence of $(\omega_{\rm eq},\, k_{\rm eq},\, \phi_k)$ for the linear axion model. Dots are numerical data and black solid lines are fitting curves (4.5).

as also can be seen in (3.10), (A.14). Therefore we have

$$\Delta(0) = \frac{1}{2}\left(1+\sqrt{(1+4\,c_2)}\right)\,, \tag{4.4}$$

with (4.2), which gives rise to $\Delta(0)=1$ for the magnetic field model and $\Delta(0)=2$ for the linear axion model.

The low T scaling of the phase ϕ_k: next let us compare (3.17) with the linear axion model result. As can be seen in figure 8, the temperature dependence of $(\omega_{\rm eq},\, k_{\rm eq},\, \phi_k)$ for the linear axion model follows

$$\frac{\omega_{\rm eq}}{2\pi T} \sim \Delta(0) + \#\,T\,, \qquad \frac{k_{\rm eq}}{T} \sim \frac{\#}{\sqrt{T}}\,, \qquad \phi_k \sim \#\,T^{3/2}\,, \tag{4.5}$$

with $\Delta(0)=2$, which is consistent with [12].[13] Thus the phase behaves differently in T in the presence of magnetic fields (3.17).

Combining (3.17) with (4.5), we may write the equilibration data of the energy diffusion at low T, depending on theories as follows

$$\omega_{\rm eq} \sim 2\pi T\,\Delta(0)\,, \qquad k_{\rm eq} \sim \sqrt{T}\,, \qquad \phi_k \sim T^{\,7/2-\Delta(0)}\,, \tag{4.6}$$

where $\Delta(0)$ depends on the theories (4.4).

Further comments on the operator scaling dimension $\Delta(0)$. The axion model (A.1)[14] can be used to study the breaking of translational invariance both explicitly ($N<5/2$) and spontaneously ($N>5/2$) in holography where the diffusion constant D becomes the energy diffusion constant [37–39, 41, 42] at $N<5/2$ and the crystal diffusion constant [40, 48] at $N>5/2$.

Unlike the explicit symmetry breaking case in [12] ($N=1$), the operator scaling dimension $\Delta(0)$ has been investigated numerically for the spontaneous symmetry breaking case in [13] ($N>5/2$). In appendix A, following a similar method presented in section 3.1, we showed how to obtain an analytic expression of $\Delta(0)$ of the axion models for general

[13] See also analytic treatment for the T-scaling (4.5) in [12].

[14] For the recent development of this model, see [47] and references therein.

JHEP02(2022)006

N, i.e., appendix A corresponds to the generalization of [12] ($N = 1$ case) to the case of general N, and we show that our analytic result is consistent with the numerical results of the previous study [13].

Note that the analytic treatment has only been performed at $N = 1$ in [12] where there is a single master field, and it is highly non-trivial to find the analytic IR green's function in the absence of the single master field.

Let us collect main equations in appendix A as follows. First, the perturbation equation (A.12) in the extremal geometry for general N is

$$\partial_\zeta^2 Z_A + \left(\frac{2\zeta}{\zeta^2-\zeta_h^2}\right)\partial_\zeta Z_A + \left(\frac{\zeta_\omega^2}{9N^2(\zeta^2-\zeta_h^2)^2} - \frac{2\left(1+6^{\frac{1-N}{N}}\frac{k^2}{m^2}\right)}{\zeta^2-\zeta_h^2}\right) Z_A = 0\,. \tag{4.7}$$

Note that, when $N = 1$ this becomes the same equation given in [12], which is constructed with the master field.

Then, near the AdS_2 boundary, equation (4.7) with (3.9) gives an operator of dimension $\Delta(k)$ (A.14) of the axion models for general N as

$$\Delta(k) = \frac{1}{2}\left(1+\sqrt{9+2^{\frac{2N+1}{N}}\,3^{\frac{1-N}{N}}\,\frac{k^2}{m^2}}\right)\,, \tag{4.8}$$

giving $\Delta(0) = 2$ (A.15) for all N, which is consistent with numerical results in [13]. For more detailed analysis about the N-dependence and a discussion comparing and contrasting the explicit and spontaneous cases, see [13].

5 Conclusion

We have studied the breakdown of hydrodynamics in the presence of magnetic fields. At low T, we checked that the equilibration frequency $\omega_{\rm eq}$ is still associated to the AdS_2 fixed point and the hydrodynamic mode at the quadratic order (2.9) is well approximated even beyond $k_{\rm eq}$, i.e., the equilibration data of the energy diffusion at low T follows

$$\omega_{\rm eq} \to 2\pi T\,\Delta(0)\,, \qquad k_{\rm eq}^2 \to \frac{\omega_{\rm eq}}{D}\,, \tag{5.1}$$

where it is first studied with the linear axion model [12]. Moreover, we also checked that (5.1) corresponds to the conjectured upper bound [12, 13] of the diffusion constant D, i.e.,

$$D \le \frac{\omega_{\rm eq}}{k_{\rm eq}^2} := v_{\rm eq}^2\,\tau_{\rm eq}\,, \tag{5.2}$$

where $v_{\rm eq} := \omega_{\rm eq}/k_{\rm eq}$ and $\tau_{\rm eq} := \omega_{\rm eq}^{-1}$ are the velocity and the timescale associated to the breakdown of hydrodynamics. The upper bound (an equality) in (5.2) is approached at low T, implying the breakdown of hydrodynamics can be used to find the upper bound of the diffusion constant D.

JHEP02(2022)006

In addition to the magnetic field case we have analytically shown $\Delta(0) = 2$ for the axion model independent of the translational symmetry breaking pattern (explicit or spontaneous), which is complementary to previous numerical results [12, 13].

Our work confirmed one of future works proposed in [12]: the results (5.1)–(5.2) continue to hold for AdS_2 fixed points supported by a different hierarchy of scales for the energy diffusion (magnetic fields).

In addition to the theory (or the hierarchy of scales)-independent property (5.1)–(5.2), we also found theory-dependent properties in $(\Delta(0), \phi_k)$ as

$$\begin{aligned} \text{Magnetic field model:} \quad & \Delta(0) = 1\,, \quad \phi_k \sim T^{5/2}\,, \\ \text{Linear axion model:} \quad & \Delta(0) = 2\,, \quad \phi_k \sim T^{3/2}\,. \end{aligned} \tag{5.3}$$

Compared with the linear axion model results, we may summarize the low T-scaling behavior of ϕ_k for the energy diffusive hydrodynamic mode as

$$\phi_k \sim T^{7/2-\Delta(0)}\,. \tag{5.4}$$

It would be interesting to check if this scaling property holds for other value of $\Delta(0)$ with different theories for the energy diffusive hydrodynamics. Moreover, it will also be interesting to investigate the scaling property of the shear diffusive hydrodynamics: only the case at finite chemical potential has been investigated so far [12]. In other words, we may fill in the empty blanks in table 1. In particular, the shear diffusion mode with magnetic fields[15] may produce interesting features because the hydrodynamic mode is the subdiffusive mode ($\omega = -iD_{\text{shear}}\, k^4$).

We also would like to make further comments on the temperature scaling of ϕ_k (5.4). A different scaling behavior, $\phi_k \sim T^{\Delta-1/2}$, has been conjectured in [12] based on the results obtained from the several diffusion modes (red parts in table 1).

One thing we can point out about this discrepancy is that the conjectured relation $\phi_k \sim T^{\Delta-1/2}$ may not be universal because we found, at least, one counter example: for instance, the energy diffusion at finite magnetic field case (5.3) cannot be matched with $\phi_k \sim T^{\Delta-1/2}$. Therefore, in order to find the relation between ϕ_k and $\Delta(0)$, it seems we need to study the temperature scaling of ϕ_k for each diffusion mode,[16] separately. In this paper, we propose that (5.4) might be the appropriate relation for the energy diffusion.

One can also try to find such a scaling relation for other diffusion cases. For instance, for the shear diffusion, one may need to further investigate the shear mode at finite magnetic field, which is left as future work below (5.4).

Although our main interest is focused on the magnetic field case and on comparing it with the previous study for the energy diffusion case: linear axion model ($N = 1$ case), it would also be interesting to see the N-dependence on the scaling relation and check if (5.4) works at $N < 5/2$ (energy diffusion case). Also, for the $N > 5/2$ case, we have the crystal diffusion instead of the energy diffusion, and it might be interesting to find

[15] The shear diffusion mode with axion charge may require further analysis due to the absence of the hydrodynamic mode.

[16] See also the footnote 9.

JHEP02(2022)006

	Axion charge	Chemical potential	Magnetic field	
Energy diffusion	$\Delta(0)=2$	$\Delta(0)=2$	$\Delta(0)=1$	$\phi_k \sim T^{7/2-\Delta(0)}$
	$\phi_k \sim T^{3/2}$	$\phi_k \sim T^{3/2}$	$\phi_k \sim T^{5/2}$	
Shear diffusion	?	$\Delta(0)=1$	?	?
	?	$\phi_k \sim T^{1/2}$	?	

Table 1. The summary for the study of the breakdown of hydrodynamics with $(\omega_{\rm eq}, k_{\rm eq})$. Red region is investigated in [12] and the blue region is considered in this paper.

the scaling behavior for the crystal diffusion as well: see the previous study [13] studying the breakdown of hydrodynamics at $N > 5/2$. We leave this direction for finding more complete scaling behavior as future work.[17]

Last but not least, it will also be interesting to figure out some phenomenological effects of the equilibration velocity ($v_{\rm eq} := \omega_{\rm eq}/k_{\rm eq}$), of which the ratio between $v_{\rm eq}$ and $v_{\rm B}$ follows

$$\frac{v_{eq}}{v_B} = \sqrt{\Delta(0)}\,, \tag{5.5}$$

where (5.1) is used with (3.20).[18] We leave these subjects as future works and hope to address them in the near future.

Acknowledgments

We would like to thank Matteo Baggioli, Wei-Jia Li for valuable discussions and correspondence. This work was supported by the National Key R&D Program of China (Grant No. 2018FYA0305800), Project 12035016 supported by National Natural Science Foundation of China, the Strategic Priority Research Program of Chinese Academy of Sciences, Grant No. XDB28000000, Basic Science Research Program through the National Research Foundation of Korea (NRF) funded by the Ministry of Science, ICT & Future Planning (NRF- 2021R1A2C1006791) and GIST Research Institute(GRI) grant funded by the GIST in 2021 and 2022. We acknowledge the hospitality at APCTP where part of this work was done. H-S. Jeong is the first author of this paper.

A Axion model

A.1 Holographic setup

We consider the axion model in (3+1) dimensions as

$$S = \int \mathrm{d}^4x\sqrt{-g}\left(R + 6 - X^N\right) \tag{A.1}$$

[17] We would like to thank the referee for pointing this out.

[18] $\tau_L = 1/\lambda_{\rm L} = 1/(2\pi T)$ is the Lyapunov time.

JHEP02(2022)006

where

$$X := \frac{1}{2}\sum_{i=1}^{2}(\partial\varphi_i)^2\,, \qquad \varphi_i = m\,x^i. \tag{A.2}$$

Note that (A.1) model allows the analytic background solution as

$$\mathrm{d}s^2 = -f(r)\,\mathrm{d}t^2 + \frac{1}{f(r)}\,\mathrm{d}r^2 + r^2(\mathrm{d}x^2+\mathrm{d}y^2)\,, \tag{A.3}$$

where

$$f(r) = r^2 - \frac{m_0}{r} + \frac{m^{2N}}{2\,(2N-3)\,r^{2N-2}}\,, \quad m_0 = r_h^3\left(1+\frac{m^{2N}}{(4N-6)\,r_h^{2N}}\right)\,, \tag{A.4}$$

here m_0 is determined by the black hole condition $f(r_h)=0$.

For the axion model (A.1), the temperature reads

$$T = \frac{1}{4\pi}\left(3\,r_h - \frac{m^{2N}}{2\,r_h^{2N-1}}\right)\,, \tag{A.5}$$

and one can study the energy diffusion mode in the following longitudinal sector

$$\begin{aligned}
&\delta g_{tt} = h_{tt}(r)\,e^{-i\,\omega\,t+i\,k\,x}\,, \quad \delta g_{tx} = h_{tx}(r)\,e^{-i\,\omega\,t+i\,k\,x}\,, \quad \delta g_{xx} = h_{xx}(r)\,e^{-i\,\omega\,t+i\,k\,x}\,,\\
&\delta g_{yy} = h_{yy}(r)\,e^{-i\,\omega\,t+i\,k\,x}\,, \quad \delta\varphi_x = \psi_x(r)\,e^{-i\,\omega\,t+i\,k\,x}\,.
\end{aligned} \tag{A.6}$$

A.2 Gauge-invariant perturbations

Following the similar procedure presented in the section 2.3, one can study the energy diffusion mode at finite axion charge m. We may have two major differences from the section 2.3.

The first difference is the diffeomorphisms and gauge-invariant[19] combinations:[20]

$$\begin{aligned}
Z_H &:= \frac{4k}{\omega}\,h_t^x + 2h_x^x - \left(2 - \frac{k^2}{\omega^2}\frac{f'(r)}{r}\right)h_y^y + \frac{2k^2}{\omega^2}\frac{f(r)}{r^2}h_t^t\,,\\
Z_A &:= \psi_x + \frac{im}{2k}\left(h_x^x - h_y^y\right)\,,
\end{aligned} \tag{A.7}$$

giving the field equations[21] for Z_H and Z_A as:

$$\begin{aligned}
0 &= A_H\,Z_H'' + B_H\,Z_H' + C_H\,Z_A' + D_H\,Z_H + E_H\,Z_A\,,\\
0 &= A_A\,Z_A'' + B_A\,Z_H'' + C_A\,Z_H' + D_A\,Z_A' + E_A\,Z_H + F_A\,Z_A\,.
\end{aligned} \tag{A.8}$$

[19] As demonstrated in [50], there could be a redundancy in the field equations due to the diffeomorphism symmetry of the theory, which can be removed by the combinations of the fields invariant under diffeomorphisms $h_{\mu\nu} \to h_{\mu\nu} + \nabla_\mu\xi_\nu + \nabla_\nu\xi_\mu$ and $\psi_x \to \psi_x + m\,\xi_x$ where $\xi_\mu = \xi_\mu(r)e^{-i\,\omega\,t+i\,k\,x}$ are gauge functions.

[20] Such a combination is not unique. Instead of (A.7), one can also have the different combination presented in [12, 49, 50] (e.g., see (E2) of [49]). Note that if we choose the gauge-invariant variables in [12, 49, 50], the equation of motions are decoupled thus can be solved independently (e.g., see (E3) of [49]). Therefore the authors in [12, 49, 50] could solve only one equation of motion unlike our case in (A.8).

[21] In (A.8), there are two equations. Substituting the second equation into the first equation, one can obtain a single equation of motion for Z_A when $N=1$.

JHEP02(2022)006

As we did in the main context of the section 2.3, we also do not write the coefficients of equations to avoid clutter.

The second difference is the AdS boundary behaviors. The asymptotic behavior of solutions depends on the symmetry breaking patterns (or the value of N) as follows.

Example 1: the explicit symmetry breaking case ($N = 1$). For the explicit symmetry breaking, the asymptotic behavior of solutions is

$$\begin{aligned} Z_H &= Z_H^{(S)}\, r^0\,(1 + \dots) + Z_H^{(R)}\, r^{-3}\,(1 + \dots)\,, \\ Z_A &= Z_A^{(S)}\, r^0\,(1 + \dots) + Z_A^{(R)}\, r^{-3}\,(1 + \dots)\,, \end{aligned} \tag{A.9}$$

where the superscripts mean that (S) is the source term and (R) is a response term.

Example 2: the spontaneous symmetry breaking case ($N = 3$). For the spontaneous symmetry breaking, they expand as

$$\begin{aligned} Z_H &= Z_H^{(S)}\, r^0\,(1 + \dots) + Z_H^{(R)}\, r^{-3}\,(1 + \dots)\,, \\ Z_A &= Z_A^{(S)}\, r^1\,(1 + \dots) + Z_A^{(R)}\, r^0\,(1 + \dots)\,. \end{aligned} \tag{A.10}$$

The remaining procedure for the determinant method is the same as those given in the section 2.3. For instance, the quasi-normal mode spectrum in figure 8 can be computed by the determinant method (2.17) with the incoming boundary condition at the horizon (2.15).

A.3 Near-horizon perturbation equations

Following the analytic method given in the section 3.1, one can also obtain the infra-red Green's function for the axion model (A.1) at general N, producing the consistent result for $N = 1$ case [12].

The extremal geometry of the axion model: one can find the extremal geometry (3.6) for axion model with

$$r_e := \frac{m}{6^{\frac{1}{2N}}}\,, \quad \zeta_h = \frac{2\pi}{3N}\delta T\,, \tag{A.11}$$

as well as the AdS_2 radius of curvature is $L^2 = 1/(3N)$.

The perturbation equation in the extremal geometry: using the same coordinate transformation (3.7) with (A.11), at leading order in ϵ, we have the single equation for $Z_A(\zeta)$, which is from the second equation in (A.8):

$$\partial_\zeta^2 Z_A + \left(\frac{2\zeta}{\zeta^2 - \zeta_h^2}\right)\partial_\zeta Z_A + \left(\frac{\zeta_\omega^2}{9N^2(\zeta^2 - \zeta_h^2)^2} - \frac{2\left(1 + 6^{\frac{1-N}{N}}\frac{k^2}{m^2}\right)}{\zeta^2 - \zeta_h^2}\right) Z_A = 0\,. \tag{A.12}$$

Note that, when $N = 1$ (A.12) becomes the same equation given in [12], which is constructed with the master field.

JHEP02(2022)006

Then, applying the AdS/CFT rule (3.11) with the boundary expansion (3.9) to the equation (A.12), the infra-red Green's function for axion model can be obtained as

$$\mathcal{G}_{\rm IR} = \frac{2\Delta(k)-1}{2}\left(\frac{3N}{\pi}\right)^{1-2\Delta(k)} T^{2\,\Delta(k)-1}\frac{\Gamma\left(\frac{1}{2}-\Delta(k)\right)\Gamma\left(\Delta(k)-\frac{i\omega}{2\pi T}\right)}{\Gamma\left(\frac{1}{2}+\Delta(k)\right)\Gamma\left(1-\Delta(k)-\frac{i\omega}{2\pi T}\right)} \tag{A.13}$$

where $\Delta(k)$ depends on the value of N

$$\Delta(k) = \frac{1}{2}\left(1+\sqrt{9+2^{\frac{2N+1}{N}}\,3^{\frac{1-N}{N}}\,\frac{k^2}{m^2}}\right). \tag{A.14}$$

Note that (A.13) at $N=1$ becomes the same infra-red Green's function [12].[22] Thus, one can notice that the axion parameter N can change two things in $\mathcal{G}_{\rm IR}$: i) the overall pre-factor; ii) $\Delta(k)$ (A.14).

Moreover, now one can find that (A.13) generates the poles as in (3.14) and the equilibration frequency ($\omega_{\rm eq} := |\omega_{n=0}|$) for general N would be

$$\frac{\omega_{\rm eq}}{2\pi T} = \Delta(0) = 2\,, \tag{A.15}$$

where $\Delta(0)=2$ for all N, which can be seen in (A.14).

References

[1] L.D. Landau and E.M. Lifshitz, *Fluid mechanics*, Pergamon Press, U.K. (1987).

[2] B. Withers, *Short-lived modes from hydrodynamic dispersion relations*, *JHEP* **06** (2018) 059 [arXiv:1803.08058] [INSPIRE].

[3] S. Grozdanov, P.K. Kovtun, A.O. Starinets and P. Tadić, *Convergence of the gradient expansion in hydrodynamics*, *Phys. Rev. Lett.* **122** (2019) 251601 [arXiv:1904.01018] [INSPIRE].

[4] S. Grozdanov, P.K. Kovtun, A.O. Starinets and P. Tadić, *The complex life of hydrodynamic modes*, *JHEP* **11** (2019) 097 [arXiv:1904.12862] [INSPIRE].

[5] M.P. Heller, A. Serantes, M. Spaliński, V. Svensson and B. Withers, *Convergence of hydrodynamic modes: insights from kinetic theory and holography*, *SciPost Phys.* **10** (2021) 123 [arXiv:2012.15393] [INSPIRE].

[6] M.P. Heller, A. Serantes, M. Spaliński, V. Svensson and B. Withers, *Hydrodynamic gradient expansion in linear response theory*, *Phys. Rev. D* **104** (2021) 066002 [arXiv:2007.05524] [INSPIRE].

[7] M.P. Heller, R.A. Janik and P. Witaszczyk, *Hydrodynamic gradient expansion in gauge theory plasmas*, *Phys. Rev. Lett.* **110** (2013) 211602 [arXiv:1302.0697] [INSPIRE].

[22] We also replace notations: $\delta T \to T$, $\zeta_\omega \to \omega$.

JHEP02(2022)006

[8] N. Abbasi and S. Tahery, *Complexified quasinormal modes and the pole-skipping in a holographic system at finite chemical potential*, *JHEP* **10** (2020) 076 [arXiv:2007.10024] [INSPIRE].

[9] A. Jansen and C. Pantelidou, *Quasinormal modes in charged fluids at complex momentum*, *JHEP* **10** (2020) 121 [arXiv:2007.14418] [INSPIRE].

[10] S. Grozdanov, *Bounds on transport from univalence and pole-skipping*, *Phys. Rev. Lett.* **126** (2021) 051601 [arXiv:2008.00888] [INSPIRE].

[11] C. Choi, M. Mezei and G. Sárosi, *Pole skipping away from maximal chaos*, arXiv:2010.08558 [INSPIRE].

[12] D. Arean, R.A. Davison, B. Goutéraux and K. Suzuki, *Hydrodynamic diffusion and its breakdown near AdS_2 quantum critical points*, *Phys. Rev. X* **11** (2021) 031024 [arXiv:2011.12301] [INSPIRE].

[13] N. Wu, M. Baggioli and W.-J. Li, *On the universality of AdS_2 diffusion bounds and the breakdown of linearized hydrodynamics*, *JHEP* **05** (2021) 014 [arXiv:2102.05810] [INSPIRE].

[14] S. Grozdanov, A.O. Starinets and P. Tadić, *Hydrodynamic dispersion relations at finite coupling*, *JHEP* **06** (2021) 180 [arXiv:2104.11035] [INSPIRE].

[15] J.M. Maldacena, *The large N limit of superconformal field theories and supergravity*, *Adv. Theor. Math. Phys.* **2** (1998) 231 [hep-th/9711200] [INSPIRE].

[16] E. Witten, *Anti-de Sitter space and holography*, *Adv. Theor. Math. Phys.* **2** (1998) 253 [hep-th/9802150] [INSPIRE].

[17] S.S. Gubser, I.R. Klebanov and A.M. Polyakov, *Gauge theory correlators from noncritical string theory*, *Phys. Lett. B* **428** (1998) 105 [hep-th/9802109] [INSPIRE].

[18] E.I. Buchbinder, S.E. Vazquez and A. Buchel, *Sound waves in $(2+1)$ dimensional holographic magnetic fluids*, *JHEP* **12** (2008) 090 [arXiv:0810.4094] [INSPIRE].

[19] E.I. Buchbinder and A. Buchel, *The fate of the sound and diffusion in holographic magnetic field*, *Phys. Rev. D* **79** (2009) 046006 [arXiv:0811.4325] [INSPIRE].

[20] J. Hansen and P. Kraus, *S-duality in AdS/CFT magnetohydrodynamics*, *JHEP* **10** (2009) 047 [arXiv:0907.2739] [INSPIRE].

[21] E.I. Buchbinder and A. Buchel, *Relativistic conformal magneto-hydrodynamics from holography*, *Phys. Lett. B* **678** (2009) 135 [arXiv:0902.3170] [INSPIRE].

[22] S.A. Hartnoll and C.P. Herzog, *Ohm's law at strong coupling: S duality and the cyclotron resonance*, *Phys. Rev. D* **76** (2007) 106012 [arXiv:0706.3228] [INSPIRE].

[23] J. Hansen and P. Kraus, *Nonlinear Magnetohydrodynamics from Gravity*, *JHEP* **04** (2009) 048 [arXiv:0811.3468] [INSPIRE].

[24] S.A. Hartnoll, P.K. Kovtun, M. Muller and S. Sachdev, *Theory of the Nernst effect near quantum phase transitions in condensed matter, and in dyonic black holes*, *Phys. Rev. B* **76** (2007) 144502 [arXiv:0706.3215] [INSPIRE].

[25] J. Hernandez and P. Kovtun, *Relativistic magnetohydrodynamics*, *JHEP* **05** (2017) 001 [arXiv:1703.08757] [INSPIRE].

[26] M. Baggioli, U. Gran and M. Tornsö, *Collective modes of polarizable holographic media in magnetic fields*, *JHEP* **06** (2021) 014 [arXiv:2102.09969] [INSPIRE].

JHEP02(2022)006

[27] A. Amoretti, D. Arean, D.K. Brattan and N. Magnoli, *Hydrodynamic magneto-transport in charge density wave states*, *JHEP* **05** (2021) 027 [arXiv:2101.05343] [INSPIRE].

[28] A. Amoretti, D.K. Brattan, N. Magnoli and M. Scanavino, *Magneto-thermal transport implies an incoherent Hall conductivity*, *JHEP* **08** (2020) 097 [arXiv:2005.09662] [INSPIRE].

[29] A. Amoretti et al., *Hydrodynamical description for magneto-transport in the strange metal phase of Bi-2201*, *Phys. Rev. Res.* **2** (2020) 023387 [arXiv:1909.07991] [INSPIRE].

[30] K.-Y. Kim, K.K. Kim, Y. Seo and S.-J. Sin, *Thermoelectric conductivities at finite magnetic field and the Nernst effect*, *JHEP* **07** (2015) 027 [arXiv:1502.05386] [INSPIRE].

[31] H.-S. Jeong, K.-Y. Kim and Y.-W. Sun, *Bound of diffusion constants from pole-skipping points: spontaneous symmetry breaking and magnetic field*, *JHEP* **07** (2021) 105 [arXiv:2104.13084] [INSPIRE].

[32] M. Blake, *Magnetotransport from the fluid/gravity correspondence*, *JHEP* **10** (2015) 078 [arXiv:1507.04870] [INSPIRE].

[33] W. Li, S. Lin and J. Mei, *Thermal diffusion and quantum chaos in neutral magnetized plasma*, *Phys. Rev. D* **100** (2019) 046012 [arXiv:1905.07684] [INSPIRE].

[34] M. Kaminski, K. Landsteiner, J. Mas, J.P. Shock and J. Tarrio, *Holographic operator mixing and quasinormal modes on the brane*, *JHEP* **02** (2010) 021 [arXiv:0911.3610] [INSPIRE].

[35] T. Faulkner, H. Liu, J. McGreevy and D. Vegh, *Emergent quantum criticality, Fermi surfaces, and AdS_2*, *Phys. Rev. D* **83** (2011) 125002 [arXiv:0907.2694] [INSPIRE].

[36] S.A. Hartnoll and D.M. Hofman, *Locally Critical Resistivities from Umklapp Scattering*, *Phys. Rev. Lett.* **108** (2012) 241601 [arXiv:1201.3917] [INSPIRE].

[37] M. Blake, *Universal diffusion in incoherent black holes*, *Phys. Rev. D* **94** (2016) 086014 [arXiv:1604.01754] [INSPIRE].

[38] M. Blake, R.A. Davison and S. Sachdev, *Thermal diffusivity and chaos in metals without quasiparticles*, *Phys. Rev. D* **96** (2017) 106008 [arXiv:1705.07896] [INSPIRE].

[39] M. Blake and A. Donos, *Diffusion and chaos from near AdS_2 horizons*, *JHEP* **02** (2017) 013 [arXiv:1611.09380] [INSPIRE].

[40] M. Baggioli and W.-J. Li, *Diffusivities bounds and chaos in holographic Horndeski theories*, *JHEP* **07** (2017) 055 [arXiv:1705.01766] [INSPIRE].

[41] K.-Y. Kim and C. Niu, *Diffusion and butterfly velocity at finite density*, *JHEP* **06** (2017) 030 [arXiv:1704.00947] [INSPIRE].

[42] H.-S. Jeong, Y. Ahn, D. Ahn, C. Niu, W.-J. Li and K.-Y. Kim, *Thermal diffusivity and butterfly velocity in anisotropic Q-Lattice models*, *JHEP* **01** (2018) 140 [arXiv:1708.08822] [INSPIRE].

[43] S. Grozdanov, K. Schalm and V. Scopelliti, *Black hole scrambling from hydrodynamics*, *Phys. Rev. Lett.* **120** (2018) 231601 [arXiv:1710.00921] [INSPIRE].

[44] A. Larkin and Y.N. Ovchinnikov, *Quasiclassical method in the theory of superconductivity*, *Sov. Phys. JETP* **28** (1969) 1200.

[45] A. Kitaev, *A simple model of quantum holography*, talks given at KITP, April 7 and May 27 (2015).

JHEP02(2022)006

[46] J. Maldacena, S.H. Shenker and D. Stanford, *A bound on chaos*, *JHEP* **08** (2016) 106 [arXiv:1503.01409] [INSPIRE].

[47] M. Baggioli, K.-Y. Kim, L. Li and W.-J. Li, *Holographic axion model: a simple gravitational tool for quantum matter*, *Sci. China Phys. Mech. Astron.* **64** (2021) 270001 [arXiv:2101.01892] [INSPIRE].

[48] M. Baggioli and W.-J. Li, *Universal bounds on transport in holographic systems with broken translations*, *SciPost Phys.* **9** (2020) 007 [arXiv:2005.06482] [INSPIRE].

[49] M. Blake, R.A. Davison, S. Grozdanov and H. Liu, *Many-body chaos and energy dynamics in holography*, *JHEP* **10** (2018) 035 [arXiv:1809.01169] [INSPIRE].

[50] R.A. Davison and B. Goutéraux, *Momentum dissipation and effective theories of coherent and incoherent transport*, *JHEP* **01** (2015) 039 [arXiv:1411.1062] [INSPIRE].

[51] M. Baggioli and O. Pujolàs, *Electron-phonon interactions, metal-insulator transitions, and holographic massive gravity*, *Phys. Rev. Lett.* **114** (2015) 251602 [arXiv:1411.1003] [INSPIRE].

[52] M. Baggioli, *Applied holography: a practical mini-course*, SpringerBriefs in Physics, Springer, Germany (2019) [arXiv:1908.02667] [INSPIRE].

JHEP02(2022)006